Materials Science and Engineering B 278 (2022) 115629

Contents lists available at ScienceDirect

Materials Science & Engineering B

journal homepage: www.elsevier.com/locate/mseb

Perpendicular magnetic properties of sputtered Pt/Co_2MnSi/MgO nanostructures

Ke Wang [a,*], Yongming Tang [a], Jian Liu [a], Caiyin You [b], Long You [c]

[a] School of Mechanical and Electronic Engineering, East China University of Technology, Nanchang 330013, China
[b] School of Materials Science and Engineering, Xi'an University of Technology, Xi'an 710048, China
[c] School of Optical and Electronic Information, Huazhong University of Science and Technology, Wuhan 430074, China

ARTICLE INFO

Keywords:
Co_2MnSi
Perpendicular magnetic properties
Interfaces
Thermal stability
Spintronic devices

ABSTRACT

Co_2MnSi (CMS) alloy is one of promising ferromagnetic electrode materials for spintronics devices. A series of CMS films sandwiched by Pt and MgO are sputtered. For the as-deposited films with in-plane anisotropy a low saturation magnetization of 494.8 ± 30.0 emu/cm^3 is determined. After annealing perpendicular magnetic anisotropy (PMA) is shown to build in the stacks with CMS thickness ranged from 2 to 3 nm. The largest saturation magnetization of 1002.0 ± 68.5 emu/cm^3 is obtained. CMS/MgO interface is found to be requisite for PMA development and Pt/CMS interface is shown to be not essential for PMA. Thermal stability is shown to be significantly improved with the insertion of Pt buffer. Strong PMA over 1×10^6 erg/cm^3 is demonstrated in a wide annealing temperature range with the insertion of 0.8 nm MgO and 4 nm Pt buffer. Our results provide some useful information for designing next generation CMS-based spintronic devices.

1. Introduction

Magnetic films with perpendicular magnetic anisotropy (PMA) are of great importance for spintronic devices such as spin-transfer-torque driven switching based magnetic random access memory (STT-MRAM) due to high thermal stability and good scalability [1,2]. The PMA allows integrating the perpendicularly magnetized film materials as ferromagnetic electrodes in perpendicular magnetic tunnel junctions (p-MTJs) [3]. From the view of practical applications, the critical current density in STT switching has to be reduced to lower the power consumption of the spintronic devices. Perpendicularly magnetized materials with high spin polarization and good thermal stability at reduced dimension are required to realize low energy consumption when used as ferromagnetic electrodes for the next generation p-MTJs [4].

Co-based Heusler alloys have gained growing interest as ferromagnetic electrode candidates for spintronics applications due to the half-metallic nature theoretically predicated perfect spin polarization [5,6]. Among them, Co_2MnSi (CMS) is one of the intensively studied materials used in such as MTJs and giant magnetoresistance devices for its high Curie temperature (985 K), wide band gap (0.4–0.81 eV) in the minority spins and large saturation magnetization (~1040 emu/cm^3) [7,8]. A high spin polarization of 93% at room temperature (*RT*) is revealed in CMS by *in situ* ultraviolet-photoemission spectroscopy [9]. A large tunneling magnetoresistance ratio up to 236% at room temperature is reported to achieve in a fully epitaxial MTJ consisting of Co2MnSi with MgO barrier [10]. A large activation barrier of 1.07 eV is optically determined for the structural magnetic transition of CMS alloy film, showing CMS possesses good thermal stability [11]. The inverse spin Hall voltage of CMS/Pt is also found to be one order larger than that in (Fe,CoFe)/Pt epitaxial films [12]. Recently, a high room temperature two-terminal magnetoresistance ratio up to 0.1% is demonstrated in semiconductor-based lateral devices with full ordered CMS, showing CMS can be used for spin injection for semiconductor-based spintronic devices [13]. Robust half-metallicity at interfaces is further confirmed in CMS-based all-full-Heusler-alloy spintronic devices [14]. However, PMA cannot be exhibited in the individual CMS alloy films. Lots of works have revealed that PMA can be built in some Co-based Heusler alloys sandwiched by MgO and heavy metals [15]. Large interfacial PMA in the order of 1×10^6 erg/cm^3 has been demonstrated to set up in the structures of thin CMS films sandwiched by Pd and MgO oxide layers, which makes the alloy attractive used in the STT-based spintronic devices [16]. PMA has been demonstrated in the structures of CMS with $MgAl_2O_4$ and even antiferromagnetic NiO oxide [17,18]. The PMA in the structures is believed to originate from the orbital hybridization or

* Corresponding author.
E-mail address: wang@ecut.edu.cn (K. Wang).

https://doi.org/10.1016/j.mseb.2022.115629
Received 16 June 2021; Received in revised form 25 December 2021; Accepted 20 January 2022
Available online 29 January 2022

alloying effects at the interfaces [19–21]. Recently, significantly enhanced extraordinary Hall effect is found in CMS with insertion of adjacent MgO layer, which may be attributed to proper Mn-O bonding at the interface [22]. In the sandwiched structures the bottom and top interfaces have shown positive contribution to the PMA of the CMS. However, it has not been clear yet which interface is the most critical factor in promoting the interfacial PMA and the thermal stability related to ultrathin CMS films has to be further improved. It is of great importance to investigate physical origin of the interfacial PMA of CMS alloy films for designing CMS-based spintronic devices.

In this work, we systematically investigate the perpendicular magnetic properties of Pt/CMS/MgO nanostructures. PMA is shown to set up in the annealed structures with CMS in the thickness range of 2–3 nm. CMS/MgO interface is revealed to be critical to develop PMA while Pt/CMS interface is not essential for promoting PMA. Thermal stability is shown to be significantly improved with the insertion of Pt buffer. For the CMS stacks with the insertion of 0.8 nm MgO and 4 nm Pt buffer strong PMA over 1×10^6 erg/cm^3 can be demonstrated in a wide annealing temperature range.

2. Experimental details

Film stacks of Si(1 0 0) substrate/Ta(10)/Pt/CMS/MgO/Pt(4) (the unit of the thickness is given in nanometers), schematically shown in Fig. 1a, were fabricated by magnetron sputtering in a chamber with a base pressure less than 1.0×10^{-5} Pa. The gas pressure was set at 0.3 Pa and the flow rate of working Ar gas was fixed at 60 sccm. The metals and MgO layers were sputtered using direct current (DC) and radio frequency (RF) power, respectively. The sputtering rates of Ta, Pt, CMS and MgO layers for the deposition were 0.2, 0.1, 0.2 and 0.2 nm/s, respectively. For the stacks the required thicknesses of CMS, Pt and MgO layers were obtained by controlling deposition time. The 10-nm-thick Ta as bottom seeding layer was pre-sputtered on Si to reduce the roughness of the substrate. After growth, 4-nm-thick Pt layer was sputtered as the capping for the protection. The sample annealing was performed in a vacuum chamber with a base pressure of 6×10^{-4} Pa at various temperatures for half an hour each. The structure of the stacks was characterized by an X-ray diffractometer (XRD, Rigaku Smartlab) with Cu Kα radiation. In-plane and out-of-plane magnetic hysteresis loops were measured using a vibrating sample magnetometer (VSM, Microsense EZ7) with the field applied along in-plane and out-of-plane directions, respectively. The extraordinary Hall effect (EHE) measurements were performed with the van der Pauw technique and the field applied perpendicular to the sample plane.

3. Results and discussion

A series of Ta(10)/Pt(6)/CMS(d)/MgO(1.2)/Pt(4) stacks with various CMS thicknesses d were fabricated. All the as-deposited stacks exhibit completely in-plane anisotropy. After annealing at 200 °C PMA appears and out-of-plane magnetization significantly develops with the measuring field applied perpendicular to the sample plane. The annealed stacks with CMS layer in the thickness range of 2–3 nm can exhibit good PMA. Fig. 1b and c show out-of-plane magnetization hysteresis loops for the Ta(10)/Pt(6)/CMS(d)/MgO(1.2)/Pt(4) stacks with CMS thickness of d = 2 and 3 nm, respectively, annealed at various temperatures. The magnetic easy axis is completely in plane for all the as-deposited films and PMA emerges only after annealing. Out-of-plane magnetization loops with high remanence are observed in two structures annealed at 200 °C. Annealing at the high temperatures leads to significantly reduced remanence, showing PMA deteriorates.

Fig. 1d shows the plot of CMS thickness dependent saturation

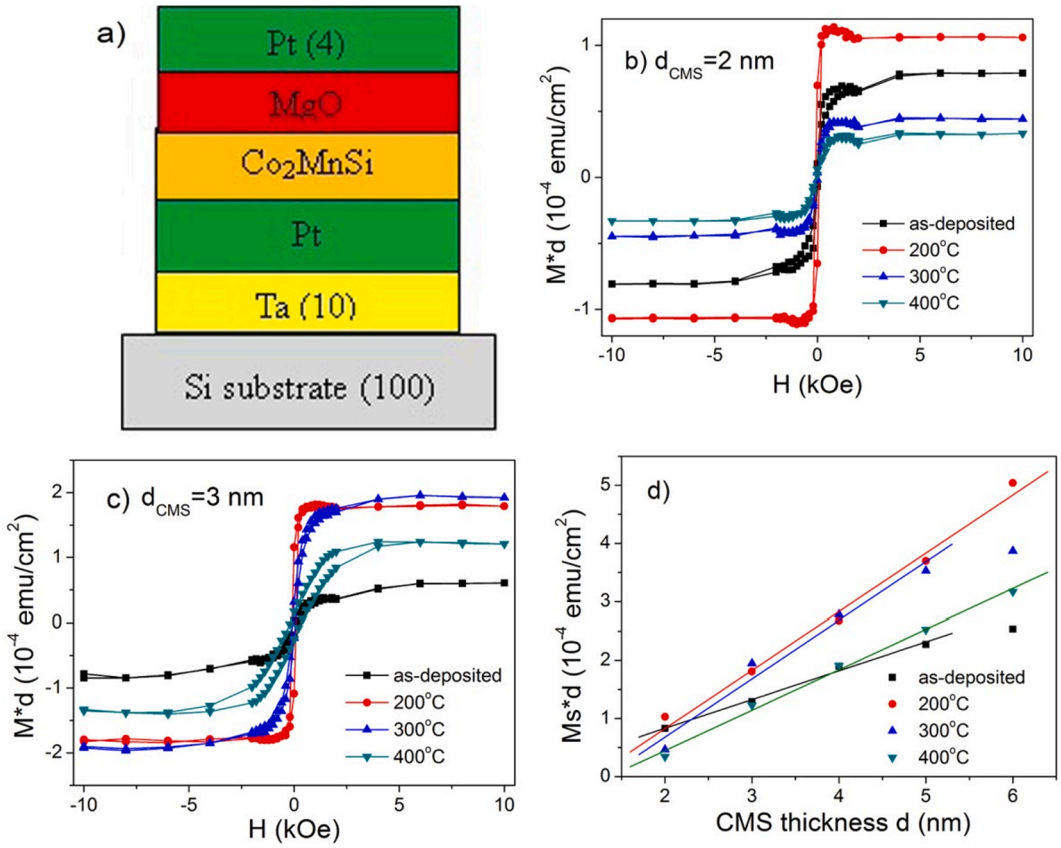

Fig. 1. a) Schematic of the stacks sputtered on Si (1 0 0) substrate. Out-of-plane magnetization hysteresis loops of the Ta(10)/Pt(6)/CMS(d)/MgO(1.2)/Pt(4) stacks annealed at various temperatures with CMS thickness d of b) 2 nm and c) 3 nm. d) Thickness dependent saturation magnetization per unit area of the stacks annealed at various temperatures.

magnetization per unit area (Ms × d) of the stacks annealed at various temperatures. The slope of the linear fitting CMS thickness dependent saturation magnetization per unit area gives the saturation magnetization of the CMS film. The thickness of magnetic dead layer (MDL) can be obtained by the intercept with the thickness axis of the linear fitting in the plot. The magnetic parameters of Pt/CMS/MgO structures derived from the fitting are listed in Table 1. For the as-deposited stacks with in-plane anisotropy the data in the thin region is used for the fitting in order to obtain the thickness of MDL. The thickness of MDL of 0.32 ± 0.22 nm is derived from the linear fitting and a low saturation magnetization of 494.8 ± 30.0 emu/cm^3 is determined. After annealing at 200 °C a large saturation magnetization of Ms = 1002.0 ± 68.5 emu/cm^3 is achieved. which is close to the bulk value of CMS (~1040 emu/cm^3) [23]. This significant increase in Ms with annealing temperature can be attributed to improved chemical orders or crystallization with the annealing [11,24,25]. Further annealing at higher temperatures leads to reduced magnetization, which can be attributed to the oxidation and degradation of PMA at high temperatures. After annealing at 200 °C the thickness of MDL is considerably increased from 0.49 ± 0.25 nm of the as-deposited films to 1.17 ± 0.29 nm. Further annealing leads to a gradual increase in the thickness of MDL. The thickness of MDL increases to 1.36 ± 0.18 nm after annealing at 400 °C. As the interfacial oxides of Mn, Co and Si in the region of CMS/MgO interface has been revealed by XPS analysis [26], the monotonic increase in the thickness of MDL with annealing temperature can be mainly attributed to the progress of the oxidation from the top CMS/MgO interface with annealing temperature.

To investigate the effects of the CMS/MgO interface, the Ta(10)/Pt (6)/CMS (3)/MgO(d)/Pt(4) stacks with various top MgO thicknesses were fabricated. Fig. 2a and b show the EHE loops of the annealed Ta (10)/Pt(6)/CMS(3)/MgO(d)/Pt(4) stacks with top MgO thickness d = 0 and 2 nm, respectively. For the structure without MgO a close-to-zero remanence is observed in the EHE loop and the magnetic easy axis nearly completely lies in the sample plane. The remanence increases with the annealing temperature and reaches a medium value of 0.49 after annealing at 350 °C. This increased remanence after annealing can be ascribed to the contribution from two interfaces of Pt/CMS. In the presence of MgO layer with thickness of 0.5 nm or thicker almost full remanence is demonstrated in the stacks after annealing at 200 °C. The remanence remains nearly constant with the annealing temperature and falls at high annealing temperatures over 300 °C. Fig. 2c shows EHE loops of Ta(10)/Pt (6)/CMS(3)/MgO(d)/Pt(4) stacks with various MgO thicknesses annealed at 250 °C. For the annealed stack without MgO layer EHE loop with zero remanence is observed and square EHE loops appear in the presence of MgO layer, showing MgO layer is crucial for the PMA development. The coercivity is shown to increase with increasing MgO thickness. This can be ascribed to sufficient oxidation, which is required to promote PMA. Fig. 2d presents typical XRD patterns of the stacks with different thickness of MgO layer before and after annealing at 300 °C for comparison. For the as-deposited Ta(10)/Pt(6)/CMS(3)/Pt(4) stack without MgO layer, no obvious peak can be recognized even after annealing. In contrast, in the presence of 0.5 nm MgO layer Pt (1 1 1) peak at 2θ = 39.5° is witnessed in the as-deposited stack. After annealing, the intensity of the peak becomes high and the position shifts towards a higher angle of 2θ = 40.6°. A strong diffraction peak centered at 2θ = 40.7° is witnessed for the annealed stack with 0.8 nm MgO layer. It suggests that CoPt alloy with a lattice constant in between face-centered-cubic Pt and Co has formed at the interfaces after annealing. It indicates MgO capping can facilitate the formation of (1 1 1)-oriented CoPt alloy in the stacks, which has been revealed to positively contribute to PMA and thermal stability [21].

Table 1
Magnetic parameters derived from the Pt/CMS/MgO structures annealed at different temperatures.

Annealing temperature	Saturation magnetization Ms (emu/cm^3)	Thickness of MDL (nm)
as-deposited	494.8 ± 30.0	0.32 ± 0.22
200 °C	1002.0 ± 68.5	1.17 ± 0.29
300 °C	1001.9 ± 122.7	1.31 ± 0.44
400 °C	695.2 ± 29.9	1.36 ± 0.18

Fig. 3 shows MgO thickness dependence of perpendicular anisotropy constant Kμ of the structures annealed in the temperature range of 200–350 °C. The perpendicular anisotropy constant Kμ is estimated using the equation Kμ=Ms(H_K − Hc)/2, where H_K is saturation field and Hc is the coercivity of the hysteresis loop with the field applied along the easy axis. The saturation field H_K can be determined from the intersection between the saturated parts of the in-plane and out-of-plane magnetization hysteresis loops For the as-deposited structure without MgO layer no PMA appears and Kμ is negative. With increasing annealing temperature Kμ increases and reaches to a small positive value of 1.28 × 10^5 erg/cm^3 after annealing at 350 °C. The contribution of the bottom and top Pt/CMS interfaces may account for this small positive value of PMA. In contrast, for the stack with the insertion of 0.5 nm MgO layer a positive Kμ of 3.4 × 10^5 erg/cm^3 is observed annealed at 200 °C and Kμ increases to 1.16 × 10^6 erg/cm^3 after annealing at 250 °C. This large Kμ achieved after annealing at 250 °C is comparable to that reported in Pt/Co_2FeAl/MgO system, which can be attributed to oxidation of CMS at the CMS/MgO interface [16,27]. The hybridization between Co/Mn and O orbitals at the top CMS/MgO interface arising from the proper oxidation results into this enhanced PMA [16,22,28]. The initially rapid increase in PMA of the stacks with MgO layers annealed in the temperature range of 200–300 °C indicates oxidation at the CMS/MgO interface is critical for the development of PMA. Further annealing at 350 °C PMA disappears and Kμ turns to be negative again.

Insets show the out-of-plane and in-plane magnetization hysteresis loops of the Ta(10)/Pt(6)/CMS(3)/MgO(d = 0, 0.8)/Pt(4) stacks after annealing at 250 °C. For the stack without MgO layer after annealing at 250 °C square loop was obtained with the field applied in the sample plane, showing the magnetic easy axis lies in the sample plane. The H_k and easy axis Hc are determined to be 2.5 kOe and 0.09 kOe, respectively. Using the saturation magnetization per unit area of 1.96 × 10^{-4} emu/cm^2 Kμ is estimated to be −0.78 × 10^6 erg/cm^3. The negative sign of Kμ indicates the easy axis is in plane. For the stack with 0.8 nm MgO after annealing at 250 °C square loop with a coercivity Hc of 0.82 kOe is achieved with the field applied perpendicular to the sample plane, showing good PMA. Using H_k of 8.0 kOe and the saturation magnetization per unit area of 1.5 × 10^{-4} emu/cm^2, Kμ is estimated to be 1.80 × 10^6 erg/cm^3. For the stacks with MgO layer of 0.8 nm or thicker large Kμ over 1 × 10^6 erg/cm^3 can be demonstrated in a wide annealing temperature range of 200–300 °C. It shows that 0.8 nm MgO is sufficient to provide optimum oxidation for the PMA of the CMS-based structures.

To examine the effects of Pt buffer on the PMA, a series of samples of Ta(10)/Pt (d)/CMS(3)/MgO(1.2)/Pt(4) with Pt buffer thickness varied from 0 to 12 nm were investigated. Fig. 4a and b show the EHE loops of Ta(10)/Pt(d = 0,2)/CMS (3)/MgO(1.2)/Pt(4) stacks annealed at various temperatures. Square EHE loop with a full remanence is obtained for the structure without Pt buffer annealed at 200 °C, showing the magnetic axis has been perpendicular to the sample plane. Annealing at higher temperatures results into significantly reduced remanence, indicating PMA seriously degrades. In contrast, with the insertion of Pt buffer large remanences can maintain in the samples annealed in a wide temperature range of 200–300 °C and the remanence considerably drops only after annealing at 350 °C. It shows Pt buffer is not essential for promoting PMA but can obviously improve thermal stability. Fig. 4c shows the EHE loops of Ta(10)/Pt(d = 0–12)/CMS(3)/MgO(1.2)/Pt(4) stacks annealed at 250 °C. Slanted EHE loop with a low remanence of 0.29 is formed in the annealed stack without Pt buffer. For the Pt-buffered stacks square EHE loops with almost full remanence appear. Once the PMA is built the coercivity is shown to decrease with increasing Pt buffer thickness. This can be explained by smoother surface of thicker Pt buffer, which is easier to facilitate the domain wall motion during the magnetic switching [29].

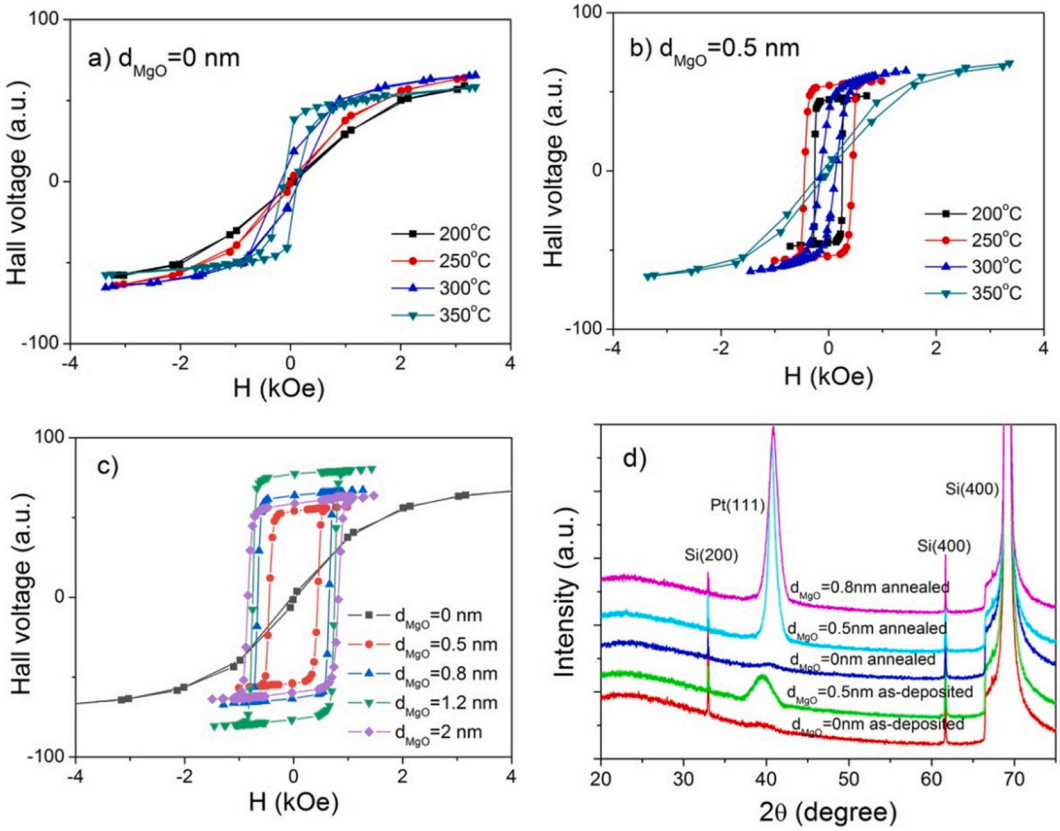

Fig. 2. EHE loops of the Ta(10)/Pt(6)/CMS(3)/MgO(d)/Pt(4) stacks annealed in the temperature range of 200–350 °C. a) MgO thickness $d = 0$ and b) $d = 0.5$ nm c) EHE loops of the Ta(10)/Pt(6)/CMS(3)/MgO(d = 0–2)/Pt(4) stacks with Mg annealed at 250 °C. d) Typical XRD patterns of the stacks with different thickness of MgO layer before and after annealing.

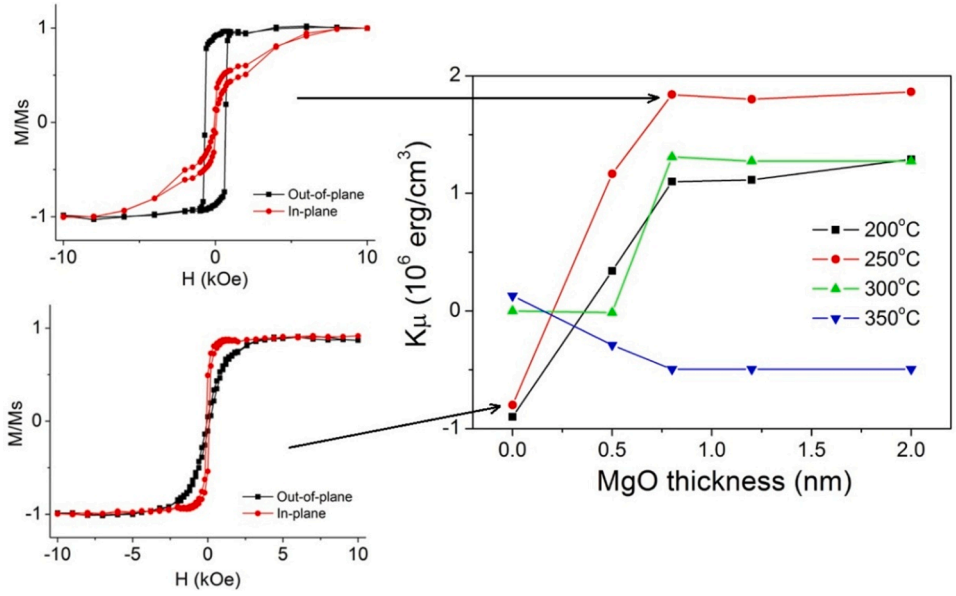

Fig. 3. MgO thickness dependence of Kμ of the Ta(10)/Pt(6)/CMS(3)/MgO (d = 0–2)/Pt (4) stacks annealed at various temperatures. Insets show out-of-plane and in-plane magnetization hysteresis loops of the Ta(10)/Pt(6)/CMS(3)/MgO(d = 0, 0.8)/Pt(4) stacks annealed at 250 °C.

The amplitude of extraordinary Hall voltage is also shown to decrease with increasing Pt buffer thickness. This can be reasonably ascribed to the shunting effect of good conductor of Pt metal. Fig. 4d presents typical XRD patterns of the stacks with different thickness of Pt buffer annealed at 300 °C. For the as-deposited Ta(10)/Pt(0,2)/CMS(3)/MgO (1.2)/Pt(4) stack without Pt or with 2 nm Pt buffer, similar Pt (1 1 1) peak at 2θ = 39.6° is witnessed. This can be ascribed to the diffraction from the Pt capping. After annealing, strong diffraction peak appears and peak position shifts towards a higher angle with increasing thickness of the Pt buffer. It, again, reflects that (1 1 1)-textured CoPt alloy

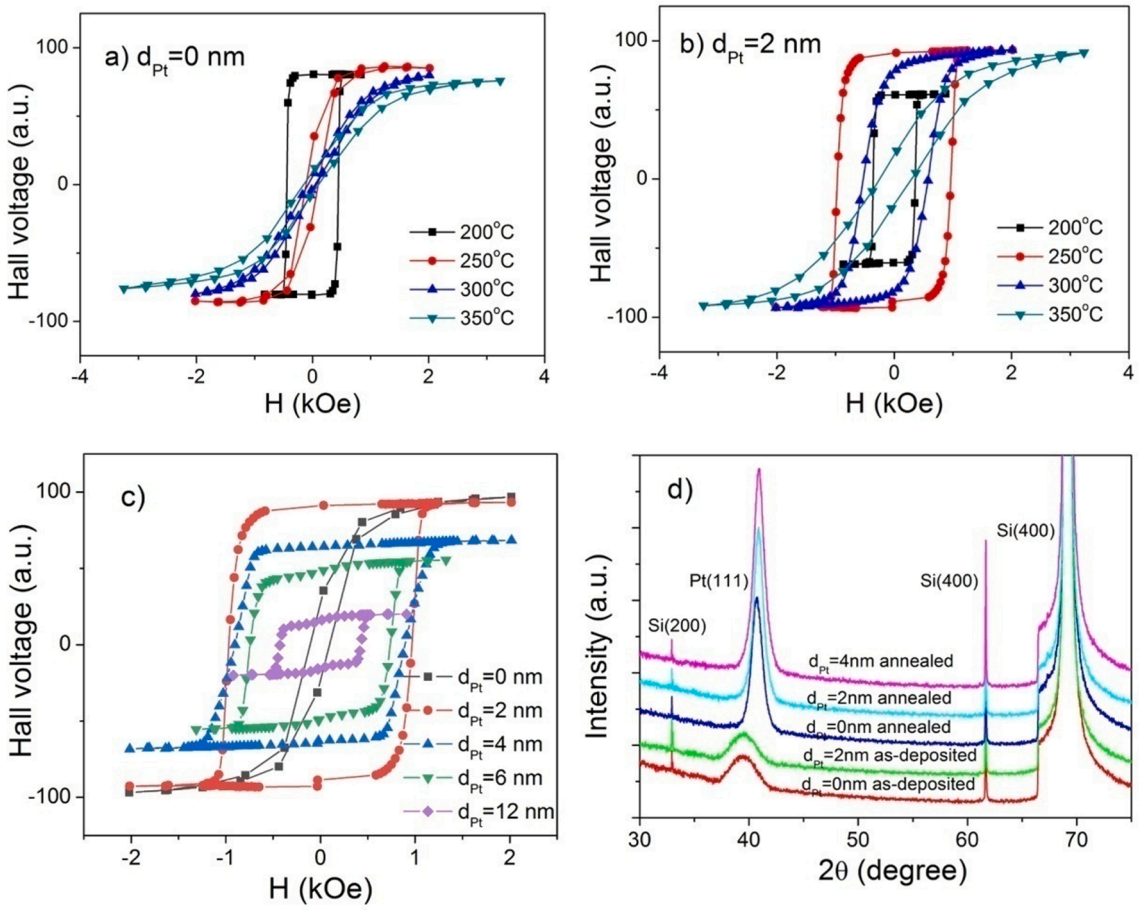

Fig. 4. EHE loops of the Ta(10)/Pt(*d*)/CMS(3)/MgO(1.2)/Pt(4) stacks annealed in the temperature range of 200–350 °C. a) Pt buffer thickness $d = 0$ and b) $d = 2$ nm c) EHE loops of the Ta(10)/Pt(d = 0–12)/CMS(3)/MgO(1.2)/Pt(4) stacks annealed at 250 °C. d) Typical XRD patterns of the stacks with different thickness of Pt buffers before and after annealing.

formed at the interfaces after annealing can promote PMA and improve the thermal stability of the stacks. Also, it indicates the top interface of CMS/MgO/Pt indeed positively contributes to PMA, accordingly, square EHE loop with large remanence can be formed in the annealed stacks without Pt buffer, as we observed.

Fig. 5 shows Pt buffer thickness dependence of Kμ of the stacks. For the stacks without Pt buffer a large Kμ of 1.22×10^6 erg/cm^3 is obtained after annealing at 200 °C and then Kμ monotonically decreases with increasing annealing temperature, showing the thermal stability is poor. For the annealed sample with insertion of 2 nm Pt buffer Kμ of 1.32×10^6 erg/cm^3 is obtained after annealing at 200 °C and the Kμ reaches a maximum of 1.73×10^6 erg/cm^3 after annealing at 250 °C. Further annealing at 300 °C PMA disappears and Kμ turns to be zero again. Insets show the out-of plane and in-plane magnetization hysteresis loops for the Ta (10)/Pt (d = 0, 4)/CMS (3)/MgO (1.2)/Pt(4) stacks annealed at 200 °C. For the stack without Pt buffer annealed at 200 °C square loop with a coercivity of 0.5 kOe is obtained with the field applied perpendicular to sample plane, showing a good PMA. Using $H_k = 6.0$ kOe and the saturation magnetization per unit area of 1.32×10^{-4} emu/cm^2 Kμ is estimated to be 1.21×10^6 erg/cm^3. For the stack with 4 nm Pt buffer annealed at 200 °C square loop with a coercivity of 0.4 kOe is witnessed with the field applied perpendicular to the sample plane. Kμ is estimated to be 1.84×10^6 erg/cm^3 using $H_k = 8.0$ kOe and the saturation magnetization per unit area of 1.45×10^{-4} emu/cm^2. A large window of annealing temperature with Kμ over 1.0×10^6 erg/cm^3 is demonstrated in the annealed samples with the insertion of 4 nm Pt buffer or thicker, indicating thermal stability of the stacks can be effectively improved by the insertion of Pt. A close-to-zero Kμ is observed for all the Pt-buffered stacks annealed at 350 °C, showing PMA deteriorates after annealing at high temperatures. The interfacial PMA induced by Pt buffer was previously found in Co-based Heusler alloy films after annealing, which mainly comes from the interfacial band hybridization [30]. Our result shows that thermal stability of the structures can be significantly improved by the insertion of Pt buffer.

To facilitate a comparison, a brief summary of magnetic parameters of annealed Co-based Heusler alloy (Co_2FeSi, $Co_2FeAlSi$ and Co_2MnSi) sandwiched by thin oxides (MgO and $MgAl_2O_4$) and heavy metals (Pt and Pd) is made in Table 2 [31–33,17]. Large saturation magnetizations ranged from 600 to 1100 emu/cm^3, comparable to the bulk value of Heusler alloy, are achieved. Strong interfacial perpendicular anisotropy density in the order of 10^6 erg/cm^3 is achieved for all the sandwiched stacks by annealing in the temperature range of 300 ~ 400 °C. The magnetic dead layer in the thickness range of 0.8 ~ 1.31 nm is obtained after annealing, which is ascribed to the interdiffusion at the interfaces during the annealing at high temperatures to promote perpendicular magnetic anisotropy.

4. Summary

In short, we investigate the perpendicular magnetic properties of the Pt/CMS/MgO structures. For the as-deposited stacks the magnetic easy axis lies in the sample plane. After annealing strong PMA is shown to build in the Pt/CMS/MgO stacks with CMS thickness ranged from 2 to 3 nm. The largest saturation magnetization close to the bulk value of CMS is achieved after annealing. No obvious PMA can be formed without MgO layers, indicating the top CMS/MgO interface is requisite for the

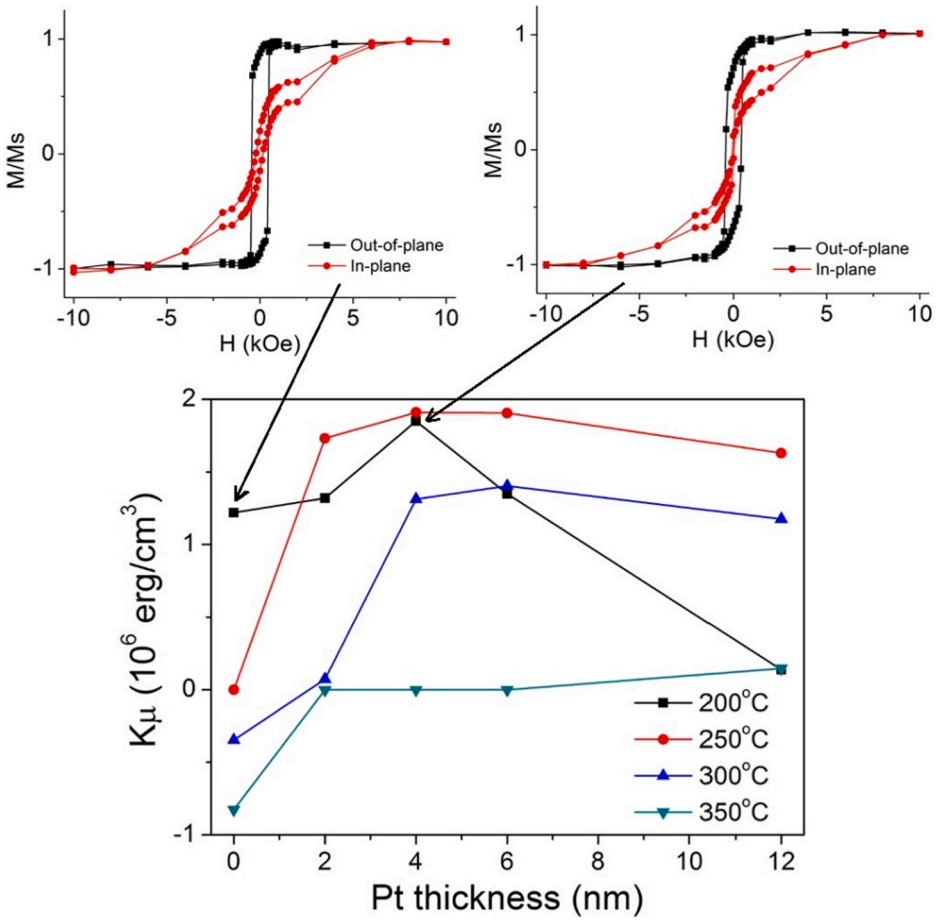

Fig. 5. Pt thickness dependence of Kμ of the Ta(10)/Pt(d = 0–12)/CMS(3)/MgO (1.2)/Pt(4) stacks. Insets show the out-of-plane and in-plane magnetization loops for the Ta(10)/Pt (d = 0, 4)/CMS(3)/MgO(1.2)/Pt(4) stacks annealed at 200 °C.

Table 2
Comparison of magnetic parameters of annealed various Co-based Heusler alloy stacks with perpendicular magnetic anisotropy.

Co-based Heusler alloy stacks	Ms (emu/cm^3)	Maximum Kμ (10^6 erg/cm^3)	t_{MDL} (nm)	RRef.
Pt(6)/Co_2FeSi/MgO(1.2)/Pt(4) annealed at 300 °C	1009 ± 41	1.2	1.19 ± 0.17	[31]
Pd(6)/Co_2FeSi/MgO(1)/Pd (2) annealed at 400 °C	1077 ± 52	1.0	0.90 ± 0.30	[32]
Pt(5)/$Co_2FeAlSi$/$MgAl_2O_4$(0.9) annealed at 340 °C	~1100	~1.3	0.8	[33]
Pd(6)/CMS/$MgAl_2O_4$(1)/Pd(6) annealed at 350 °C	~600	~0.6	1.6	[17]
Pt(6)/CMS/MgO(0.5)/Pt (4) annealed at 300 °C	1002 ± 123	1.3	1.31 ± 0.44	This work

PMA development. The thermal stability of the stacks is shown to be significantly improved by Pt/CMS interface. It shows that stacks with 0.8 nm MgO and 4 nm Pt buffer layers can exhibit strong PMA over 1 × 10^6 erg/cm^3 in a wide temperature range. (111)-textured Pt or CoPt alloy are identified, which may be correlated to enhanced PMA and improved thermal stability of the stacks. Our results provide some useful information for the next generation CMS-based spintronic devices.

Declaration of Competing Interest

The authors declare that they have no known competing financial interests or personal relationships that could have appeared to influence the work reported in this paper.

Acknowledgements

This work was supported by the National Natural Science Foundation of China (Grant No. 51961004).

References

[1] S. Ikeda, K. Miura, H. Yamamoto, K. Mizunuma, H.D. Gan, M. Endo, S. Kanai, J. Hayakawa, F. Matsukura, H. Ohno, A perpendicular-anisotropy CoFeB–MgO magnetic tunnel junction, Nat. Mater 9 (9) (2010) 721–724.
[2] J. Xu, C.L. Chien, Voltage Controlled Spin-Orbit Torque Switching in W/CoFeB/MgO, Appl. Phys. Lett 118 (2021), 052409.
[3] Y.P. Kabanov, R.D. Shull, C. Zheng, P.W.T. Pong, D.B. Gopman, Asymmetric magnetization reversal of the Heusler alloy Co_2FeSi as free layer in an CoFeB/MgO/Co_2FeSi magnetic tunnel junction, Appl. Surf. Sci. 536 (2021), 147672.
[4] Z.C. Wen, H. Sukegawa, S. Mitani, K. Inomata, Perpendicular magnetization of Co_2FeAl full-Heusler alloy films induced by MgO interface, Appl. Phys. Lett 98 (2011), 242507.
[5] A. Semiannikova, Y.A. Perevozchikova, V.Y. Irkhin, E.B. Marchenkova, P. S. Korenistov, V.V. Marchenkov, Electronic, magnetic and galvanomagnetic properties of Co-based Heusleralloys: Possible states of a half-metallic ferromagnet and spin gapless semiconductor, AIP Advances 11 (2021), 015139.
[6] S.A. Sofi, D.C. Gupta, High Pressure-Temperature study on thermodynamics, half-metallicity, transport, elastic and structural properties of Co-based Heusler alloys: A first-principles study, J. Solid State Chem. 284 (2020) 121178, https://doi.org/10.1016/j.jssc.2020.121178.
[7] S. Amari, R. Mebsout, S. Méçabih, B. Abbar, B. Bouhafs, First-principle study of magnetic, elastic and thermal properties of full Heusler Co_2MnSi, Intermetallics 44 (2014) 26–30.
[8] A. Hirohata, W. Frost, M. Samiepour, J.-Y. Kim, Perpendicular Magnetic Anisotropy in Heusler Alloy Films and Their Magnetoresistive Junctions, Materials 11 (1) (2018) 105, https://doi.org/10.3390/ma11010105.

[9] M. Jourdan, J. Minar, J. Braun, A. Kronenberg, S. Chadov, B. Balke, A. Gloskovskii, M. Kolbe, H.J. Elmers, G. Schonhense, H. Ebert, C. Felser, M. Klaui, Direct observation of half-metallicity in the Heusler compound Co_2MnSi, Nat. Commun 5 (2014) 3974.
[10] T. Ishikawa, H.X. Liu, T. Taira, K. Matsuda, T. Uemura, M. Yamamoto, Influence of film composition inCo2MnSi electrodes on tunnel magnetoresistance characteristics of Co_2MnSi/MgO/Co_2MnSi magnetic tunnel junctions, Appl. Phys. Lett 95 (2009), 232512.
[11] K.e. Wang, S. Dong, Z. Xu, Y.a. Huang, Crystallization and magnetic properties in amorphous Co_2MnSi alloy films, Mater. Lett. 180 (2016) 140–143.
[12] Y. Sasaki, S. Sugimoto, Y. K. Takahashi, S. Kasai, Spin injection efficiency through the pumping in epitaxial Co_2MnSi/Pt thin film, AIP Advances10 (2020) 085311.
[13] K. Kudo, M. Yamada, S. Honda, Y. Wagatsuma, S. Yamada, K. Sawano, K. Hamaya, Room-temperature two-terminal magnetoresistance ratio reaching 0.1% in semiconductor-based lateral devices with L21-ordered Co_2MnSi, Appl. Phys. Lett. 118 (2021), 162404.
[14] B. Pradines, L. Calmels, R. Arras, Robustness of the Half-Metallicity at the Interfaces in Co_2MnSi-Based All-Full-Heusler-Alloy Spintronic Devices, Phys. Rev. Appl. 15 (2021), 034009.
[15] M.S. Gabor, M. Nasui, A. Timar-Gabor, Perpendicular magnetic anisotropy in Pt/Co-based full Heusler alloy/MgO thin-film structure, Phys. Rev. B 100 (2019), 144438.
[16] H.R. Fu, C.Y. You, Y. Li, K. Wang, N. Tian, Interfacial contributions to perpendicular magnetic anisotropy in Pd/Co_2MnSi/MgO trilayer films, J. Phys. D Appl. Phys 49 (2016), 195001.
[17] K.L. Wen, X.W. Xiu, J. Jiang, Y. He, F.Z. Huang, S.Y. Wang, Perpendicular magnetic anisotropy of Pd/Co_2MnSi/MgAl2O4/Pd structure films, J. Phys. D: Appl. Phys 52 (2019), 485005.
[18] J. Jiang, X.W. Xiu, K.L. Wen, W.T. Cao, Y. He, S.Y. Wang, Perpendicular magnetic anisotropy of Pd/Co55Mn25Si20/NiO/Pd sputtering film, J. Magn. Magn. Mater. 505 (2020), 166709.
[19] J.P. Hadorn, H. Sukegawa, T. Ohkubo, S. Mitani, K. Hono, Microstructural evolution of perpendicular magnetization films with an ultra-thin Co_2FeAl/MgAl2O4(001) structure, Acta Materialia 145 (2018) 306–315.
[20] A. Conca, A. Niesen, G. Reiss, B. Hillebrands, Evolution of the interfacial perpendicular magnetic anisotropy constant of the Co_2FeAl/MgO interface upon annealing, J. Phys. D: Appl. Phys 51 (2018), 165303.
[21] A. Basha, H.R. Fu, G. Levi, G. Leitus, A. Kovács, C.Y. You, A. Kohn, Interface alloying of ultra-thin sputter-deposited Co_2MnSi films as a source of perpendicular magnetic anisotropy, J. Magn. Magn. Mater. 489 (2019), 165367.
[22] H.R. Fu, L. Ma, N. Tian, C.Y. You, K. Wang, The enhancement of anomalous Hall effect by inserting MgO layer in perpendicular anisotropic Pd/Co_2MnSi/MgO/Pd films, AIP Adv. 8 (2018), 055804.
[23] M. Obaida, K. Westerholt, H. Zabel, Magnetotransport properties of Cu_2MnAl, Co_2MnGe, and Co_2MnSi Heusler alloy thin films: From nanocrystalline disordered state to long-range-ordered crystalline state, Phys. Rev. B 84 (2011), 184416.
[24] X. Yang, R. Liu, X. Shen, F. Song, Magnetic properties and BSA adsorption of nano-Fe-embedded $BaFe_{12}O_{19}$ porous microfibers via organic gel-thermal selective reduction process, J. Sol-Gel Sci. Technol. 63 (1) (2012) 8–15.
[25] X.C. Yang, Z. Wang, M.X. Jing, R.J. Liu, F.Z. Song, X.Q. Shen, Magnetic nanocomposite Ba-ferrite/α-iron hollow microfifiber: A multifunctional 1D space platform for dyes removal and microwave absorption, Ceram. Int. 40 (2014) 15585–15594.
[26] A. McFadden, N. Wilson, T. Brown-Heft, D. Pennachio, M. Pendharkar, J.A. Logan, C.J. Palmstrøm, Interface formation of epitaxial MgO/Co_2MnSi(001) structures: Elemental segregation and oxygen migration, J. Magn. Magn. Mater. 444 (2017) 383–389.
[27] Z.C. Wen, H. Sukegawa, S. Mitani, K. Inomata, Perpendicular magnetization of full-Heusler alloy films induced by MgO interface, Appl. Phys. Lett 98 (2011), 242507.
[28] K. Munira, J. Romero, W.H. Butler, Achieving perpendicular anisotropy in half-metallic Heusler alloys for spin device applications, J. Appl. Phys 115 (2014) 17B731.
[29] S.P. Pati, M. Al-Mahdawi, Y. Shiokawa, M. Sahashi, Y. Endo, Effect of a platinum buffer layer on the magnetization dynamics of sputter deposited YIG polycrystalline thin films, IEEE Trans. Magn. 53 (11) (2017) 1–5.
[30] N. Nakajima, T. Koide, T. Shidara, H. Miyauchi, H. Fukutani, A. Fujimori, K. Iio, T. Katayama, M. Nývlt, Y. Suzuki, Perpendicular magnetic anisotropy caused by interfacial hybridization via enhanced orbital moment in Co/Pt Multilayers: magnetic circular x-ray dichroism study, Phys. Rev. Lett 81 (1998) 5229–5232.
[31] K. Wang, X.P. Xiao, Z.K. Xu, L. Wu, J. Liu, Annealing effects and perpendicular magnetic properties of sputtered Co_2FeSi alloy films, Appl. Phys. A 127 (2021) 725.
[32] K.e. Wang, Y. Tang, X. Xiao, J. Liu, Effects of Pd- and Ta-buffer layer on magnetic and interfacial perpendicular properties of sputtered Co_2FeSi/MgO heterostructures, Surf. Eng 37 (4) (2021) 497–504.
[33] Y. Wu, X. Xu, L.u. Li, Z. Wang, J. Miao, Y. Jiang, Perpendicular magnetic anisotropy of Pt/$Co_2FeAl0.5Si0.5$/MgAl2O4 trilayers, Phys. Status Solidi A 213 (10) (2016) 2780–2784.